DOI: 10.31534/engmod.2025.2.ri.03a
Professional paper
Received: 04.07.2025.

# Modelling of Elastohydrodynamic Journal Bearing with Ultra-Small Clearances

**Jingpeng Wu**[(1)], **Yongbin Zhang***[(1)]

[(1)] *College of Mechanical Engineering, Changzhou University, Changzhou, Jiangsu Province, CHINA*

* *Corresponding author: e-mail: engmech1@sina.com*

## SUMMARY

*This paper presents the numerical calculation for the elastohydrodynamic journal bearing with ultra-small clearances (with the eccentricity ratios approaching unity), where in a local small area only the physically adsorbed layer is present, while in the other areas the sandwich film is present. It is shown that both the adsorbed layer and the elastic deformation of the surface strongly influence the performance of the bearing. For a given operating condition, the surface elastic deformation causes significant reductions in both the maximum hydrodynamic pressure and the load of the bearing, while it significantly increases the minimum clearance (for a given eccentricity ratio) and the friction coefficient. The surface elastic deformation also increases film stiffness. These effects are strongly dependent on the fluid-surface interaction; the stronger the fluid-surface interaction, the more significant the effect of the surface elastic deformation. The present study shows the considerable benefit of the adsorbed layer formed by the strong fluid-surface interaction in increasing the bearing minimum clearance (for a given load or a given eccentricity ratio) and reducing the friction coefficient of the bearing when the surface elastic deformation is involved.*

**KEYWORDS:** *adsorbed layer; elastic deformation; friction coefficient; hydrodynamics; journal bearing; load; pressure.*

## 1. INTRODUCTION

Journal bearings are very important components that carry load by reducing friction and wear [1]. Hydrodynamic lubrication theories have been extensively developed for them by considering surface elasticity [2, 3], fluid rheological behavior [4, 5], film thermal effect [6, 7] and surface roughness [8, 9] etc. Those theories are based on the continuum assumption and ignore the molecule layers of fluid on the surface. Indeed, they may be valid for relatively large surface clearances, such as on the scales of 1-10 $\mu m$ or more. However, in modern industry, of the extremely heavy loads and high fluid-film temperatures, the hydrodynamic fluid film may be

difficult to form and it may break down in a journal bearing, resulting in surface seizure [10]. This case represents an extremely severe operating condition in which the eccentricity ratio approaches unity.

When the surface clearance is ultra-low, the physically adsorbed boundary layer plays a vital role in a journal bearing. Actually, in most areas, a sandwich film is present, which consists of both the physically adsorbed layer and the continuum fluid film [11]. The sandwich film flow is, in fact, multiscale [11]. Obviously, for this case, the conventional hydrodynamic lubrication theory [12] fails.

Shao et al. [13] studied the hydrodynamic journal bearing with ultra-small clearances by assuming rigid bearing surfaces and using a multiscale approach. In their study, the eccentricity ratio approached unity, so that the physically adsorbed layer occurred locally, while in the other areas a sandwich film was present. They calculated the bearing loads for varying eccentricity ratios and found that the fluid-surface interaction strongly influences the bearing load capacity.

The present study is a further development of Shao et al. [13]. It computationally investigates the hydrodynamic journal bearing with ultra-small clearances, considering the surface elastic deformation, the magnitude of which may be comparable to the surface clearance. In addition to the carried loads, the shear stresses on the surfaces and the bearing friction coefficient are calculated based on the non-continuum flow theory. Several new mechanisms are revealed concerning the combined effects of the adsorbed layer and the surface elastic deformation. These findings are of significant interest for the design of the current type of journal bearing.

## 2. DESCRIPTION OF THE BEARING

The studied bearing is shown in Figure 1. The operating regime of this bearing is different from the conventional type [12], since the surface clearance is ultra-low, so that the effect of the adsorbed layer becomes significant. The magnitude of the surface elastic deformation resulting from hydrodynamic pressures may often be comparable to the surface clearance. On the other hand, the adsorbed layer formed due to the fluid-surface interaction should have a pronounced influence on the bearing performance. The coupling effect of these two important factors in the journal bearing has not yet been revealed and is addressed in the present study. This bearing operates under heavy loads and/or high fluid-film temperatures. Its load-carrying and friction mechanisms are therefore crucial for preventing surface damage. The local, purely physically adsorbed layer behaves as a non-continuum medium: its rheology, flow regime and friction are substantially different from conventional understanding. In the other areas, the effect of the adsorbed layer still plays a role. The flow in this bearing is multiscale, and the film rheologies are highly mixed.

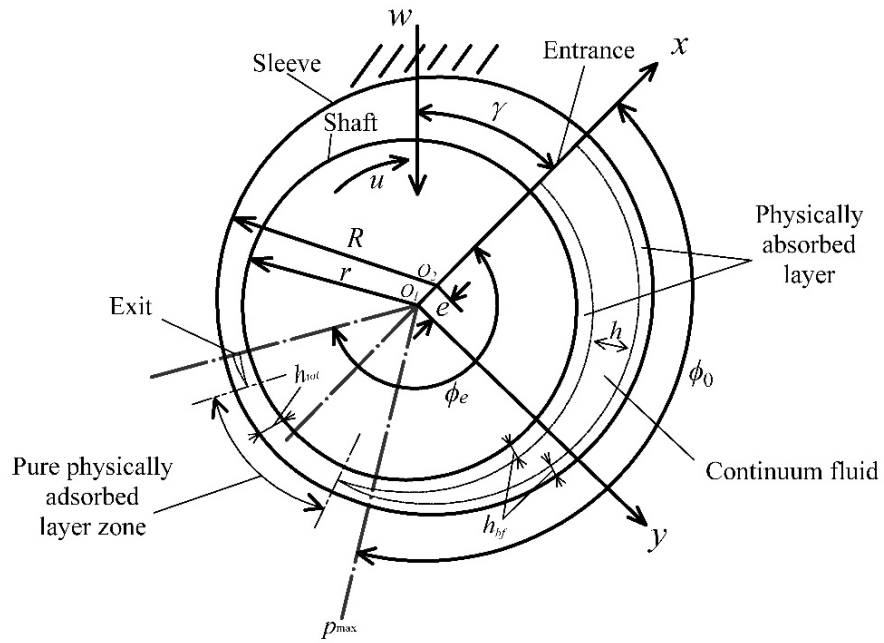


**Fig. 1** *The studied journal bearing with ultra-small clearance involving the effects of the adsorbed layer and the surface elastic deformation*

## 3. MATHEMATICAL ANALYSIS

The flow of the pure adsorbed layer is described by the nanoscale non-continuum flow equation [14]. The sandwich film flow is described by Zhang's multiscale flow equations [11], which are closed and explicit in form. These equations make the present study feasible, without requiring massive computational sources.

The detailed analysis of the present mixed-film flow has been presented by Shao et al. [13]; for brevity, it is not repeated here. Unlike the former study, the present work considers the elastic deformation of the bearing surfaces and formulates the surface separation in the bearing as:

$$h_{tot}(\phi) = c + e\cos\phi - \frac{2}{\pi E_v}\int_0^{\phi_e} p(\phi_s)\ln(r\phi - r\phi_s)^2 d\phi_s \quad \textbf{(1)}$$

where $c = R - r$, $\phi$ is the angular coordinate, $p$ is the film pressure, and $E_v$ is the equivalent Young's modulus of elasticity of the two bearing surfaces. The continuum fluid film thickness is: $h = h_{tot} - 2h_{bf}$.

### 3.1 CALCULATING THE SURFACE ELASTIC DEFORMATION

In Eq. (1), there is the following term:

$$\Theta(\phi_j) = -\frac{2r}{\pi E_v}\int_0^{\phi_e} p(\phi_s)\ln(r\phi_j - r\phi_s)^2 d\phi_s \quad \textbf{(2)}$$

Since the mathematical formulation for the exact pressure distribution is not possible, Eq. (2) can only be numerically approximated by interpolating the pressures in each discretized section $[\phi_{i-1}, \phi_i]$ using the nodal pressures $p_{i-1}$ and $p_i$. Here, when calculating $\Theta(\phi_j)$ by Eq. (2), we approximately take the pressures in the section area $[\phi_{i-1}, \phi_i]$ as the nodal pressure $p_{i-1}$. Thus, Eq. (2) can be expressed as:

$$\Theta(\phi_j) \approx \sum_{i=1}^{N-1} C_{ji} p_i \tag{3}$$

where:

$$\begin{aligned} C_{ji} &= -\frac{2r}{\pi E_v} \int_{r\cdot\frac{\phi_i+\phi_{i-1}}{2}}^{r\cdot\frac{\phi_i+\phi_{i+1}}{2}} ln(r\phi_j - r\phi_s)^2 d\phi_s \\ &= -\frac{2r}{\pi E_v} [ln(r\cdot\frac{\phi_i+\phi_{i+1}}{2} - r\phi_j)^2 (r\cdot\frac{\phi_i+\phi_{i+1}}{2} - r\phi_j) \\ &\quad - ln(r\cdot\frac{\phi_i+\phi_{i-1}}{2} - \phi_j)^2 (r\cdot\frac{\phi_i+\phi_{i-1}}{2} - r\phi_j) - r(\phi_{i+1} - \phi_{i-1})] \end{aligned} \tag{4}$$

Here, $\phi_{i-1}$, $\phi_i$ and $\phi_{i+1}$ are, respectively, the angular coordinates of the $(i\text{-}1)^{th}$, $i^{th}$ and $(i+1)^{th}$ discretized points.

### 3.2 SHEAR STRESS AND FRICTION COEFFICIENT

In the present bearing, due to the absence of interfacial slippage, and according to the multiscale flow theory [11], the shear stress on the sleeve surface in the multiscale flow area is [11]:

$$\tau_h = \frac{v_A - \frac{\partial p}{r\partial\phi} D \sum_{j=1}^{n-1} \frac{j\Delta_{j-1}}{\eta_{line,j-1}}}{\sum_{j=1}^{n-1} \frac{\Delta_{j-1}}{\eta_{line,j-1}}} + \frac{\partial p}{r\partial\phi} D \tag{5}$$

The shear stress on the shaft surface in the multiscale flow area is given by [11]:

$$\tau_s = -\frac{v_B - u - \frac{\partial p}{r\partial\phi} D \sum_{j=1}^{n-1} \frac{j\Delta_{j-1}}{\eta_{line,j-1}}}{\sum_{j=1}^{n-1} \frac{\Delta_{j-1}}{\eta_{line,j-1}}} - \frac{\partial p}{r\partial\phi} D \tag{6}$$

where $D$ is the fluid molecule diameter, $n$ is the equivalent number of the fluid molecules across the adsorbed layer thickness, $v_A$ and $v_B$ are, respectively, the velocities of the continuum fluid film on the boundaries adjacent to the sleeve and shaft surfaces, $\Delta_{j-1}$ is the separation between the $j^{th}$ and $(j\text{-}1)^{th}$ fluid molecules across the adsorbed layer thickness, and $\eta_{line,j-1}$ is the local viscosity between the $j^{th}$ and $(j\text{-}1)^{th}$ fluid molecules across the adsorbed layer thickness. According to the multiscale flow theory [11]:

$$v_A = \frac{\partial p}{r\partial\phi} D\sum_{j=1}^{n-1}\frac{j\Delta_{j-1}}{\eta_{line,j-1}} + \frac{u\eta}{2\eta\sum_{j=1}^{n-1}\frac{\Delta_{j-1}}{\eta_{line,j-1}} + h}\sum_{j=1}^{n-1}\frac{\Delta_{j-1}}{\eta_{line,j-1}} - \frac{\partial p}{r\partial\phi}\left(\frac{h}{2}+Dn\right)\sum_{j=1}^{n-1}\frac{\Delta_{j-1}}{\eta_{line,j-1}} \quad (7)$$

and

$$v_B = \frac{\partial p}{r\partial\phi} D\sum_{j=1}^{n-1}\frac{j\Delta_{j-1}}{\eta_{line,j-1}} + \frac{u}{\frac{2\eta}{h}\sum_{j=1}^{n-1}\frac{\Delta_{j-1}}{\eta_{line,j-1}} + 1}\left(\frac{\eta}{h}\sum_{j=1}^{n-1}\frac{\Delta_{j-1}}{\eta_{line,j-1}} + 1\right) - \frac{\partial p}{r\partial\phi}\left(\frac{h}{2}+Dn\right)\sum_{j=1}^{n-1}\frac{\Delta_{j-1}}{\eta_{line,j-1}} \quad (8)$$

Assume that $\eta_{line,j} / \eta_{line,j+1} = q_0^{\gamma}$, where $q_0$ (>1) is the average value of $\Delta_{j+1}/\Delta_j$ and $\gamma$ is constant [11]; Then, we have:

$$\sum_{j=1}^{i}\frac{\Delta_{j-1}}{\eta_{line,j-1}} = \frac{\Delta_{n-2}\left[q_0^{(1+\gamma)(i-n+2)} - q_0^{-(n-2)(1+\gamma)}\right]}{\eta_{line,n-2}\left(q_0^{(1+\gamma)}-1\right)}, \quad \text{for } i=1, 2, \ldots, (n\text{-}1) \quad (9)$$

$$\sum_{j=1}^{i}\frac{j\Delta_{j-1}}{\eta_{line,j-1}} = \frac{\Delta_{n-2}}{\eta_{line,n-2}}\left[\frac{q_0^{(2-n)(1+\gamma)} - q_0^{(1+\gamma)(i-n+2)}}{(q_0^{1+\gamma}-1)^2} + \frac{iq_0^{(1+\gamma)(i-n+2)}}{q_0^{1+\gamma}-1}\right], \quad \text{for } i=1, 2, \ldots, (n\text{-}1) \quad (10)$$

where $\eta_{line,j-2}$ is the local viscosity within the adsorbed layer adjacent to the continuum fluid film,taken as $\eta$.

Substituting Eqs. (7), (9) and (10) into Eq. (5) and rearranging yields:

$$\tau_h = \frac{\eta u}{\frac{2\Delta_{n-2}[q_0^{(1+\gamma)} - q_0^{-(n-2)(1+\gamma)}]}{q_0^{1+\gamma}-1} + h} - \frac{\partial p}{r\partial\phi}\left(\frac{h}{2}+D(n-1)\right) \quad (11)$$

Substituting Eqs. (8)-(10) into Eq. (6) and rearranging yields:

$$\tau_s = \frac{\eta u}{\frac{2\Delta_{n-2}[q_0^{(1+\gamma)} - q_0^{-(n-2)(1+\gamma)}]}{q_0^{1+\gamma}-1} + h} + \frac{\partial p}{r\partial\phi}\left(\frac{h}{2}+D(n-1)\right) \quad (12)$$

By using a forward difference for $\partial p/\partial\phi$, the shear stresses, respectively, on the sleeve and shaft surfaces on the $j^{th}$ discretized point in the multiscale flow area are formulated, respectively, as:

$$\tau_{h,j} = \frac{\eta u}{\frac{2\Delta_{n-2}\left[q_0^{(1+\gamma)} - q_0^{-(n-2)(1+\gamma)}\right]}{q_0^{1+\gamma}-1} + h_j} - \frac{p_j - p_{j-1}}{r\Delta\phi}\left(\frac{h_j}{2}+D(n-1)\right) \quad (13)$$

and

$$\tau_{s,j}=\frac{\eta u}{\dfrac{2\Delta_{n-2}\left[q_0^{(1+\gamma)}-q_0^{-(n-2)(1+\gamma)}\right]}{q_0^{1+\gamma}-1}+h_j}+\frac{p_j-p_{j-1}}{r\Delta\phi}\left(\frac{h_j}{2}+D(n-1)\right) \tag{14}$$

According to the nanoscale non-continuum flow theory [15], in the pure adsorbed layer zone, the shear stresses on the sleeve and shaft surfaces are, respectively, given by:

$$\tau_h=D\frac{\partial p}{r\partial\phi}\left[n_{00}-\frac{\left(\dfrac{l\Delta_{l-1}}{\eta_{line,l-1}}\right)_{avr,n_{00}-1}}{\left(\dfrac{\Delta_l}{\eta_{line,l}}\right)_{avr,n_{00}-1}}\right]-\frac{u}{(n_{00}-1)\left(\dfrac{\Delta_l}{\eta_{line,l}}\right)_{avr,n_{00}-1}} \tag{15}$$

and

$$\tau_s=-\frac{u+D(n_{00}-1)\dfrac{\partial p}{r\partial\phi}\left(\dfrac{l\Delta_{l-1}}{\eta_{line,l-1}}\right)_{avr,n_{00}-1}}{(n_{00}-1)\left(\dfrac{\Delta_l}{\eta_{line,l}}\right)_{avr,n_{00}-1}} \tag{16}$$

where $n_{00}$ is the equivalent number of the fluid molecules across the entire surface separation in the pure adsorbed layer zone, and the definitions of the other parameters remain the same as above.

The value of $n_{00}$ should vary with the surface separation $h_{tot}$ in the pure adsorbed layer zone, which itself varies with the angular coordinate $\phi$. The value of $n_{00}$ is determined according to the following equation:

$$h_{tot}=n_{00}D+2\frac{\Delta_{im}\left(q_0^{-\frac{n_{00}-1}{2}}-1\right)}{q_0^{-1}-1}=c+e\cos\phi-\frac{2r}{\pi E_v}\int_0^{\phi_e}p(\phi_s)\ln(r\phi-r\phi_s)^2d\phi_s \tag{17}$$

where $\Delta_{im}$ is the separation between neighboring fluid molecules across the surface separation at the median plane of the surface separation in the pure adsorbed layer zone, and $n_{00}$ should be an odd number [15]. Note that $n_{00}$ may vary with $\phi$ in the pure adsorbed layer zone.

For the pure adsorbed layer zone, the following equations are used [16]:

$$(n_{00}-1)\left(\frac{\Delta_l}{\eta_{line,l}}\right)_{avr,n_{00}-1}=\frac{\Delta_{im}}{\eta_{line,im}}\left(\frac{q_0^{\frac{n_{00}-1}{2}(\gamma+1)}-1}{q_0^{\frac{n_{00}-1}{2}(\gamma+1)}-q_0^{\frac{n_{00}-3}{2}(\gamma+1)}}+\frac{q_0^{\frac{3-n_{00}}{2}(\gamma+1)}-q_0^{(\gamma+1)}}{1-q_0^{(\gamma+1)}}\right) \tag{18}$$

and

$$(n_{00}-1)\left(\frac{l\Delta_{-1}}{\eta_{line,l-1}}\right)_{avr,n_{00}-1}=\frac{\Delta_{im}}{\eta_{line,im}}\left\{\frac{1}{q_0^{(\frac{n_{00}-1}{2}-1)(\gamma+1)}}\left(\frac{1-q_0^{\frac{n_{00}-1}{2}(\gamma+1)}}{(q_0^{\gamma+1}-1)^2}+\frac{\frac{n_{00}-1}{2}q_0^{(\gamma+1)\frac{n_{00}-1}{2}}}{q_0^{\gamma+1}-1}\right)+\right.$$
$$\left.+\frac{n_{00}-1}{2}\frac{q_0^{(\gamma+1)(1-\frac{n_{00}-1}{2})}-q_0^{\gamma+1}}{1-q_0^{\gamma+1}}+\frac{1-q_0^{-(\gamma+1)\frac{n_{00}-1}{2}}}{\left[q_0^{-(\gamma+1)}-1\right]^2}+\frac{\frac{n_{00}-1}{2}q_0^{-(\gamma+1)\frac{n_{00}-1}{2}}}{q_0^{-(\gamma+1)}-1}\right\} \quad (19)$$

where $\eta_{line,im}$ is the local viscosity at the median plane of the surface separation in the pure adsorbed layer zone.

The friction forces per unit contact length on the sleeve and shaft surfaces are, respectively, given by:

$$F_h=r\Delta\phi\sum_{j=1}^{N}\tau_{h,j} \quad (20)$$

and

$$F_s=r\Delta\phi\sum_{j=1}^{N}\tau_{s,j} \quad (21)$$

The friction coefficients on the sleeve and shaft surfaces are, respectively, given by:

$$f_h=\frac{|F_h|}{w} \quad \text{and} \quad f_s=\frac{|F_s|}{w} \quad (22)$$

### 3.3 NUMERICAL SOLUTION PROCEDURE

Figure 2 shows the numerical solution procedure. $p^{(0)}$, $h^{(0)}$ and $w^{(0)}$ are, respectively, the hydrodynamic pressure distribution, continuum film thickness distribution, and bearing load for rigid surfaces; $\vartheta$ is the relaxation factor.

The software for numerical calculation was developed by us in MATLAB. It is independent of any commercial finite element analysis software. The flowchart of our code is shown in Figure 2.

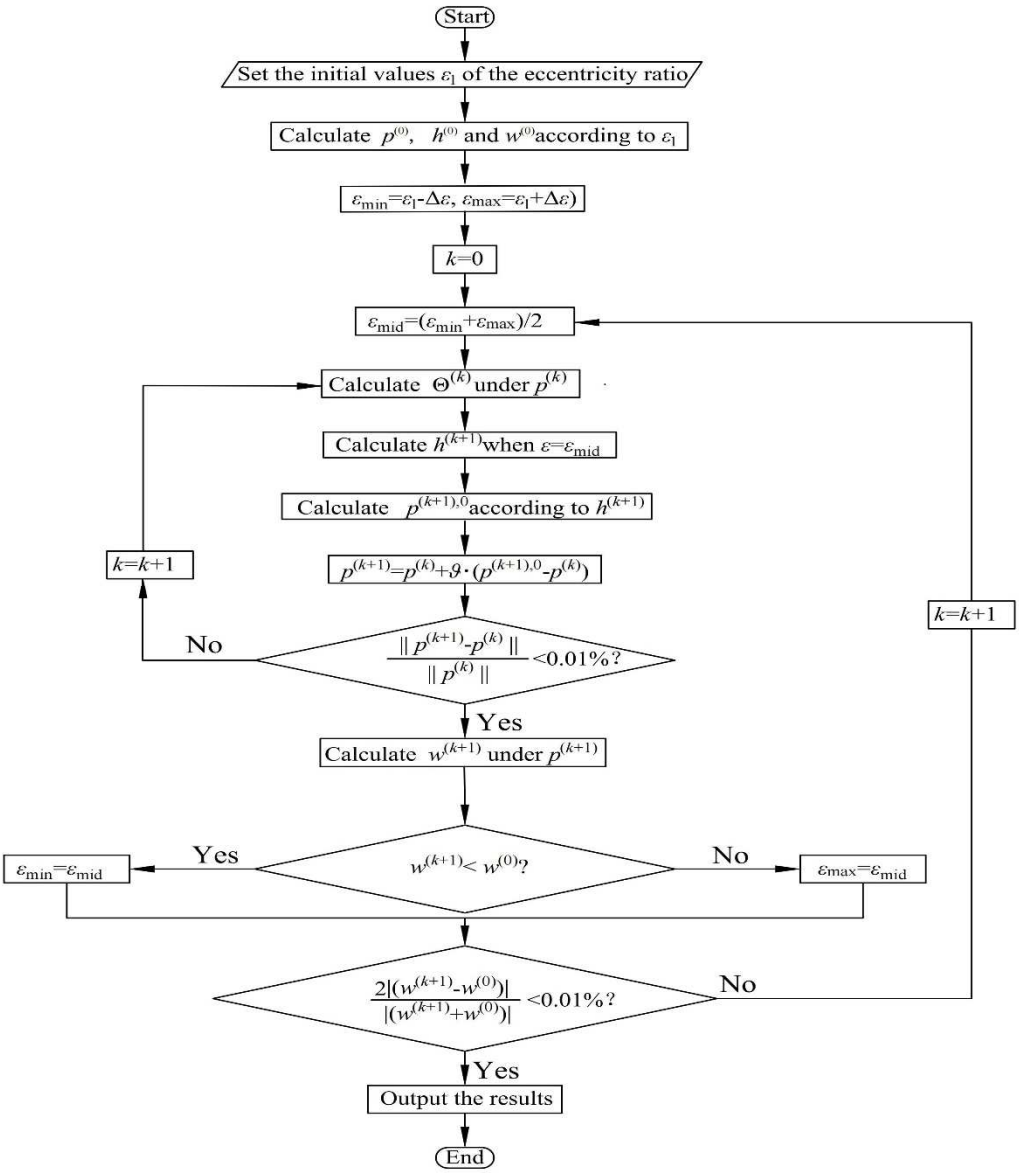


**Fig. 2** *The numerical chart for determining the eccentricity ratio for the given load $w^{(0)}$, considering the surface elastic deformation*

## 4. OPERATIONAL PARAMETER VALUES

Both the fluid piezo-viscous effect and the fluid compressibility under pressure were considered, as formulated by Shao et al. [13]. The weak, medium and strong fluid-bearing surface interactions were also taken into account, and the corresponding characteristic parameter values for these interactions were provided by Shao et al. [13].

In the calculations, the following input parameter values were used:

$$\Delta x/D=\Delta_{n-2}/D=0.15,\ D=0.5\ nm,\ r=10\ mm,\ c=3\ \mu m,\ \eta_a=0.01 Pa\cdot s,\ E_v=2.09\times10^{11} Pa,$$

$$N=2000,\ \vartheta=0.2$$

where $N$ is the total number of discretized points in the entire lubricated area, $\Delta x$ is the separation between the neighboring fluid molecules in the circumferential direction within the adsorbed layer, and $\eta_a$ is the fluid viscosity at ambient pressure.

## 5. CALCULATION RESULTS

### 5.1 PRESSURE DISTRIBUTIONS AND BEARING LOADS FOR DIFFERENT CONTACT REGIMES

Figure 3(a) presents the film pressure distributions for different fluid-surface interactions when $\varepsilon = e/c = 0.999$, $u = 0.1\ \mu m/s$, and the bearing surfaces are elastically deformed. As the fluid-surface interaction becomes stronger, the film pressures, particulary in the pure adsorbed layer zone, rise significantly. However, compared with the pressures for the assumed rigid surfaces shown in Figure 3(b), the influence of fluid-surface interaction on film pressure is notably reduced when the bearing surfaces are elastically deformed. For weak interaction, Figure 3(a) also indicates that the bearing load obtained for the elastic surfaces is slightly smaller than that predicted by the classical model [12].

For a given $\varepsilon$ and a specified fluid-surface interaction, Figure 4 shows that the effect of sliding speed on film pressure is weaker for elastic bearing surfaces than for rigid ones, although the general trend remains similar. Figures 5(a)-(c) demonstrate that surface elastic deformation has a pronounced effect on the pressures in the pure adsorbed layer zone, but only a minor influence in the hydrodynamic regions. The surface elastic deformation reduces the film pressures, particularly under strong fluid-surface interaction. In contrast, for weak interactions, the effect is much less significant because the generated pressures, and consequently, the magnitudes of the surface elastic deformation, are smaller.

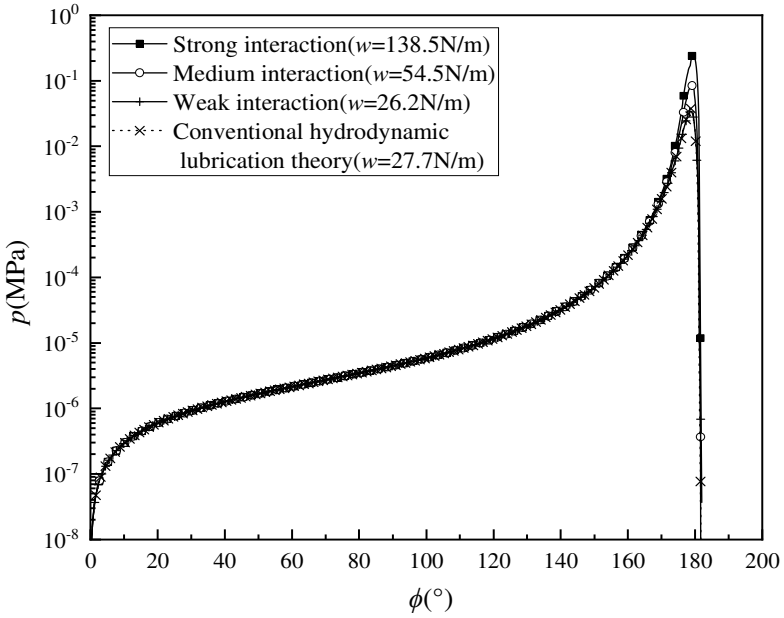


**(a)** *For elastic bearing surfaces*

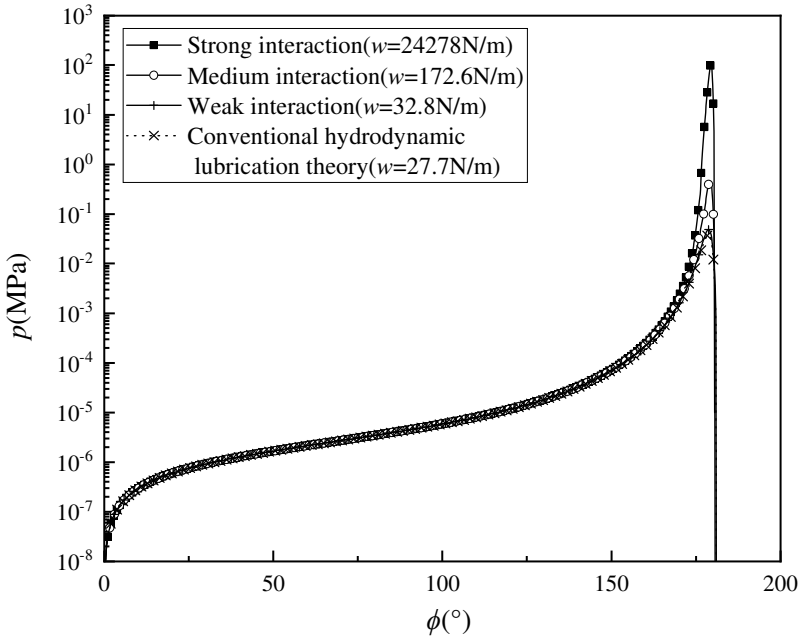


**(b)** *For the assumed rigid bearing surfaces [13]*

**Fig. 3** *Film pressure distributions for the elastically deformed and assumed rigid bearing surfaces for $\varepsilon = 0.999$ and u = 0.1 μm/s*

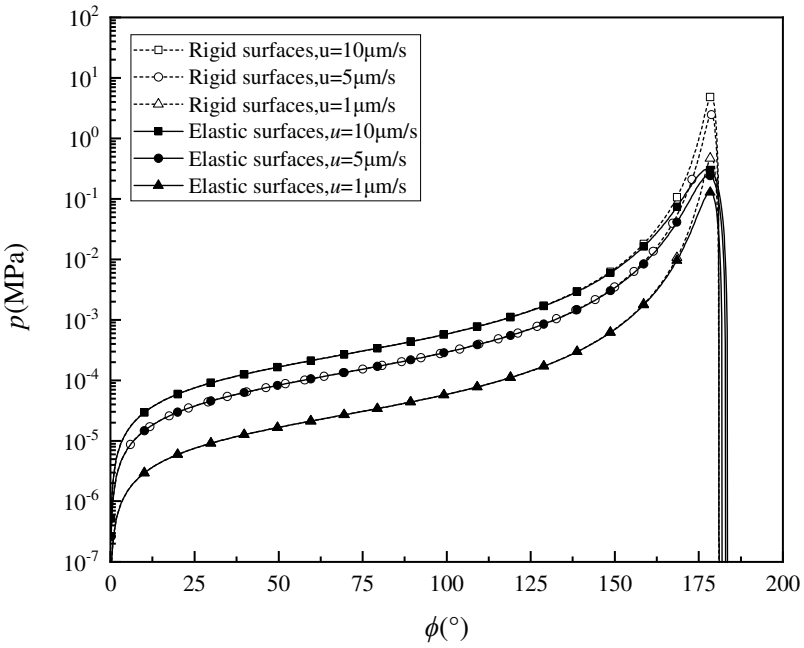


**Fig. 4** *Film pressure distributions for different speeds for the elastically deformed and assumed rigid bearing surfaces for $\varepsilon = 0.999$ and the weak fluid-surface interaction*

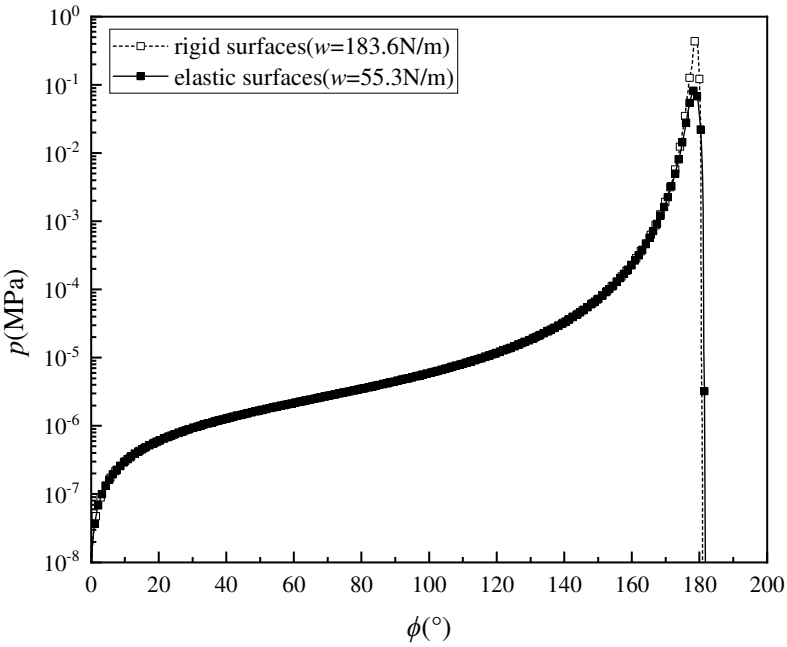


**(a)** *For strong interaction and $\varepsilon = 0.9977$*

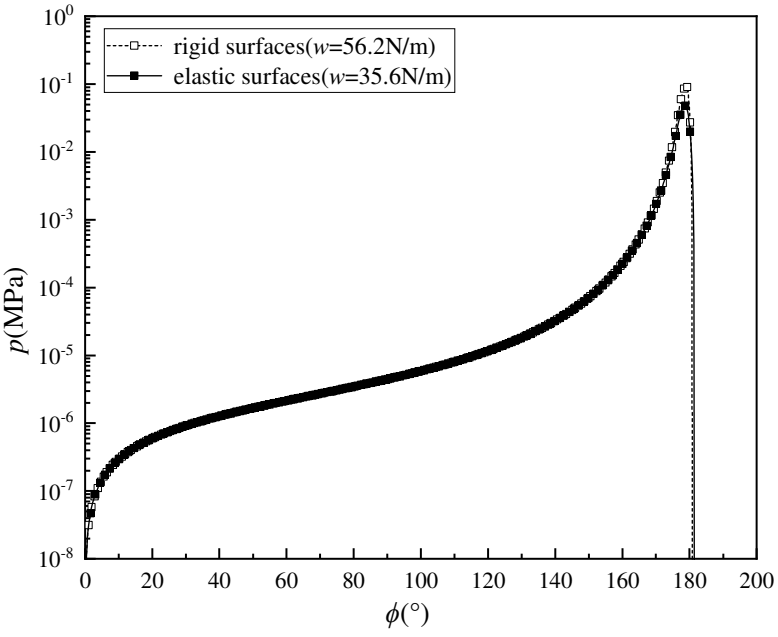


**(b)** *For medium interaction and $\varepsilon = 0.985$*

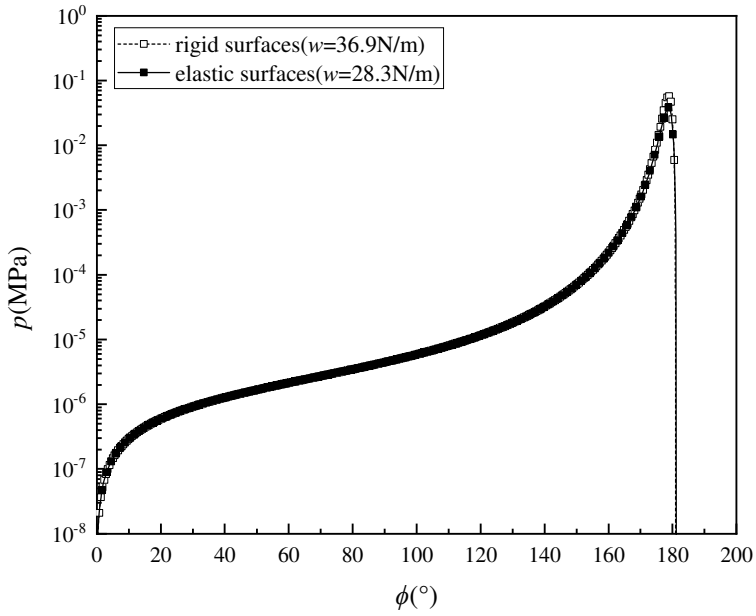


**(c)** *For weak interaction and $\varepsilon = 0.9991$*

**Fig. 5** *Film pressure distributions for the elastically deformed and assumed rigid bearing surfaces for $u = 0.1\ \mu m/s$*

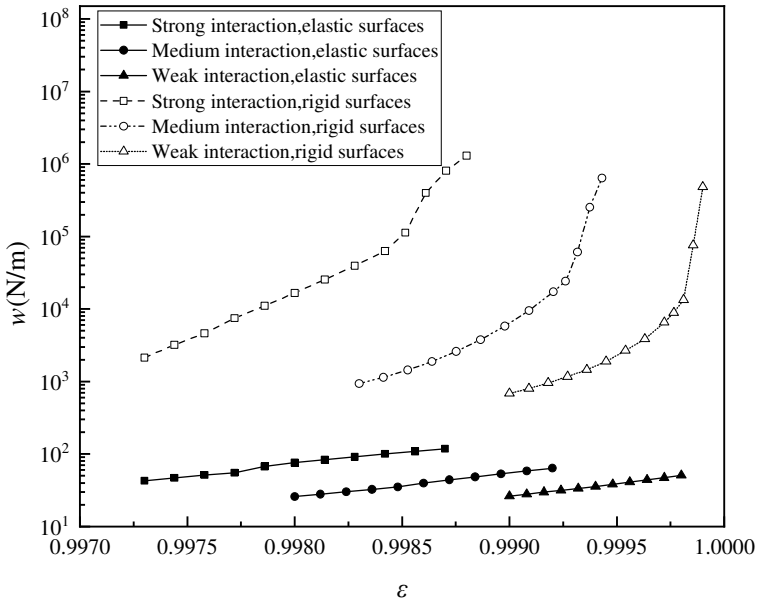


**Fig. 6** *Loads per unit contact length carried by the bearing for different contact regimes when $u = 0.1\ \mu m/s$*

Figure 6 shows that for the sliding speed $u = 0.1\ \mu m/s$ and a large eccentricity ratio ($\varepsilon > 0.997$), surface elastic deformation reduces the bearing load by approximately two orders of magnitude compared to the assumed rigid surfaces, particularly for stronger fluid-surface interactions. For

elastically deformed bearing surfaces, the influence of the fluid-surface interaction on the bearing load is significantly weaker than for rigid surfaces. In the elastic contact regime, the rate of increase of the bearing load with eccentricity ratio is considerabely smaller than in the rigid contact regime, regardless of the fluid-surface interaction.

## 5.2 SURFACE SEPARATION PROFILES AND FILM STIFFNESS FOR DIFFERENT CONTACT REGIMES

For the same sliding speed and the same eccentricity ratio, Figures 7(a)-(c) show that the surface separations in the pure adsorbed layer zone, including the minimum surface clearance for the elastically deformed bearing surfaces, are significantly greater than those for the assumed rigid bearing surfaces, especially for a stronger fluid-surface interaction.

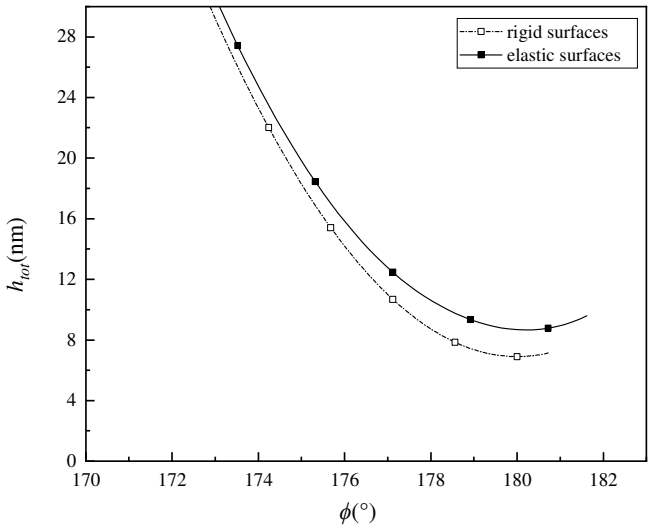


**(a)** *For strong interaction and $\varepsilon = 0.9977$*

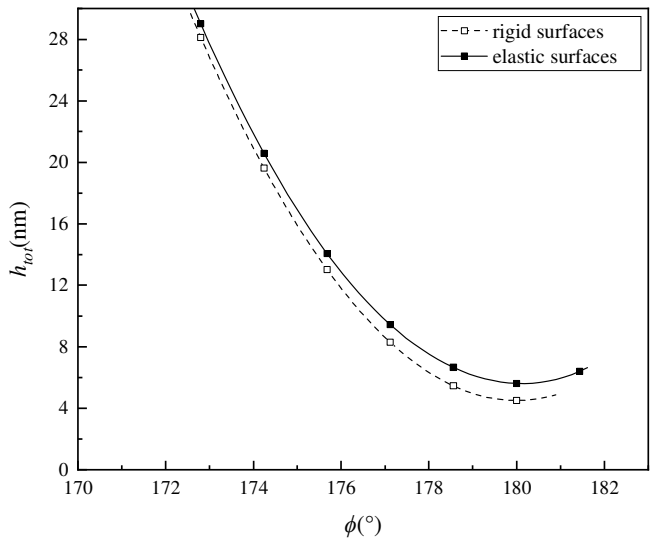


**(b)** *For medium interaction and $\varepsilon = 0.9985$*

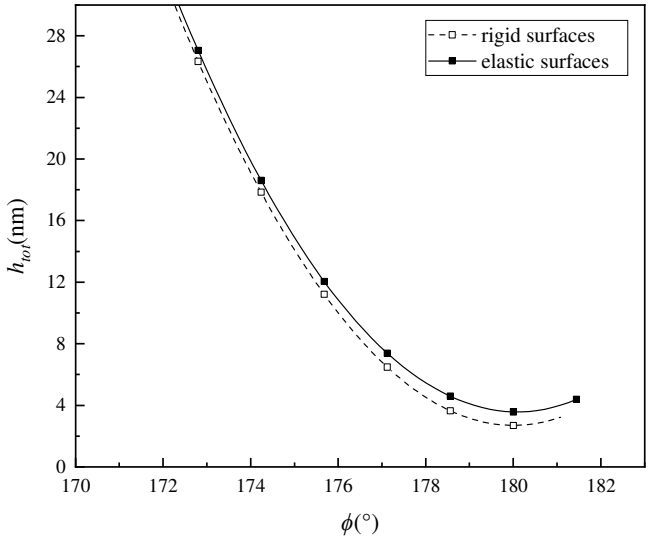


**(c)** *For weak interaction and $\varepsilon = 0.9991$*

**Fig. 7** *Influence of the surface elasticity on the surface separation profiles for u = 0.1 μm/s*

Figure 8 shows that for $u = 0.1\ \mu m/s$ and $\varepsilon = 0.999$, because of the fluid-surface interaction, the surface separations in the pure adsorbed layer zone, including the minimum bearing clearance, are significantly increased compared with the case of the rigid bearing surfaces. This effect is significant for the strong fluid-surface interaction, which increases the minimum bearing clearance by nearly one time. This is due to the much higher pressures and the consequently much greater magnitudes of the surface elastic deformation in the pure adsorbed layer zone caused by the strong fluid-surface interaction, as shown above.

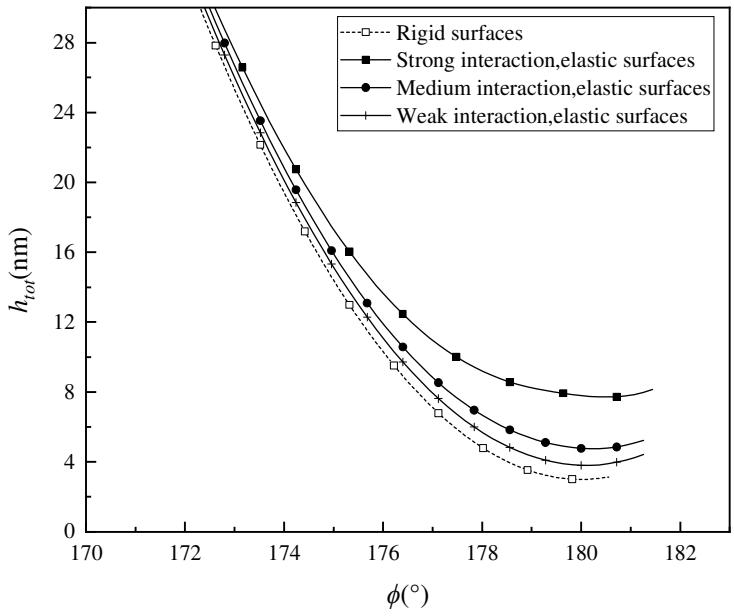


**Fig. 8** *Effect of the fluid-surface interaction on the surface separation profiles when u = 0.1 μm/s,*

*$\varepsilon$ = 0.999 and the bearing surfaces are elastically deformed*

Figure 9 shows that when the bearing surfaces are elastically deformed, the slope of the variation of the minimum surface clearance $h_{tot,min}$ with the eccentricity ratio $\varepsilon$ is significantly reduced compared with the case of the rigid bearing surfaces when the values of $\varepsilon$ approach unity. This is especially the case when the fluid-surface interaction is strong, where a residual film is seemingly present in the pure adsorbed layer zone for $\varepsilon$ approaching unity. It is shown that for the same very large value of $\varepsilon$, a stronger fluid-surface interaction gives a significantly greater value of the minimum bearing clearance when the bearing surfaces are elastically deformed.

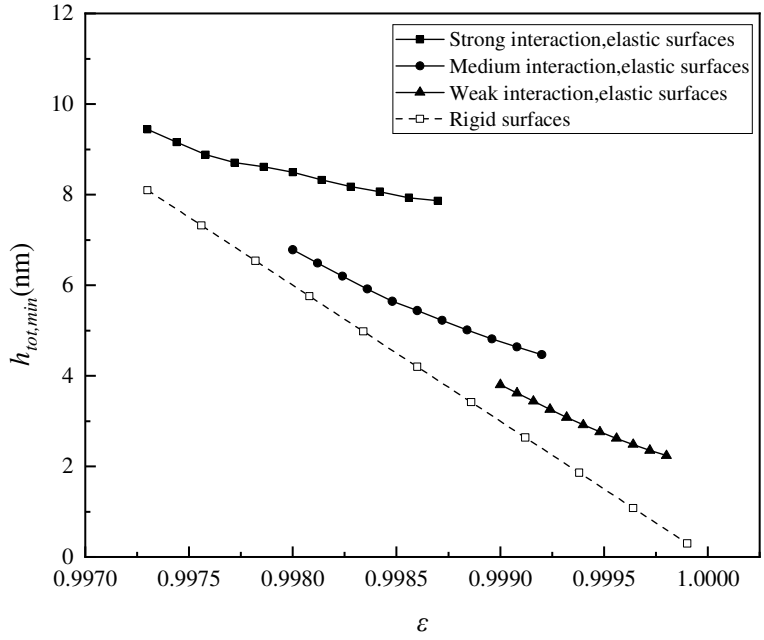


**Fig. 9** *Variations of the minimum surface clearance ($h_{tot,min}$) with the eccentricity ratio ($\varepsilon$) for different contact regimes when u = 0.1 $\mu$m/s and the values of $\varepsilon$ approach unity*

Figure 10 shows the load ($w$) versus minimum bearing clearance ($h_{tot,min}$) curves for different contact regimes when $u$ = 0.1 $\mu m/s$. The magnitudes of the slopes of these curves represent the film stiffness for different contact regimes. The surface elasticity results in considerably increased film stiffness, especially for the strong fluid-surface interaction when $h_{tot,min}$ is 1 on the nanometer scale. That is, for the same load, the value of $h_{tot,min}$ for the elastically deformed surfaces is considerably greater than that for the assumed rigid surfaces especially, for the strong fluid-surface interaction; alternatively, for the same minimum surface clearance, the bearing load for the elastically deformed surfaces is considerably larger than for the rigid surfaces, especially for the strong fluid-surface interaction. These results show the very significant benefits of both surface elastic deformation and strong fluid-surface interaction in improving the bearing performance.

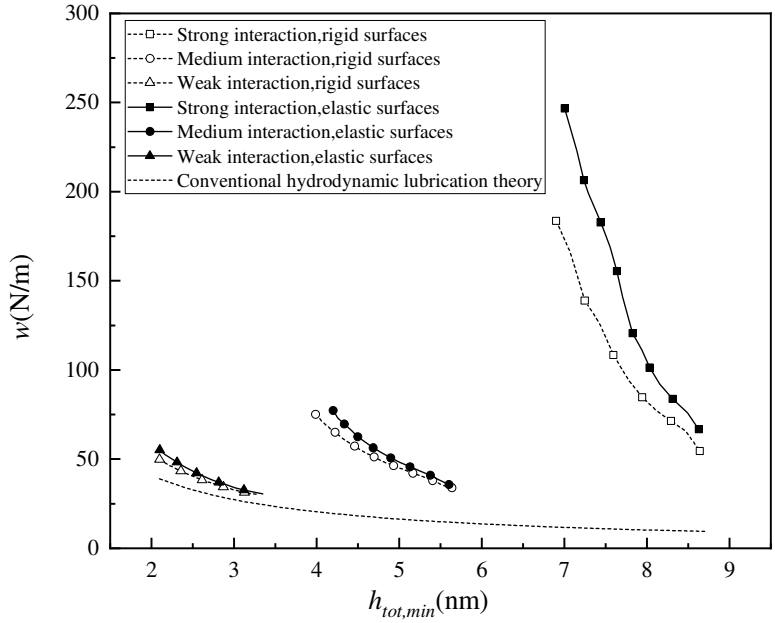


**Fig. 10** *Load versus minimum bearing clearance curves for different contact regimes when u = 0.1 μm/s*

### 5.3 SURFACE SHEAR STRESSES AND FRICTION COEFFICIENTS OF THE BEARING FOR DIFFERENT CONTACT REGIMES

Figures 11(a)-(c) show the distributions of the shear stress $\tau_h$ on the sleeve in the pure adsorbed layer zone for different fluid-surface interactions when $\varepsilon = 0.999$ and $u = 0.1\ \mu m/s$. For a given fluid-surface interaction, the surface elasticity results in significant reductions in the magnitudes of the shear stress on the sleeve in the pure adsorbed layer zone, especially for a stronger fluid-surface interaction. However, when the adsorbed layer effect (with different fluid-surface interactions) is considered, the shear stress magnitudes on the sleeve in the pure adsorbed layer zone are considerably greater than those classically calculated [12], even when the bearing surfaces are elastically deformed. Figures 12(a)-(c) show the same effects on the magnitudes of the shear stress $\tau_s$ on the shaft in the pure adsorbed layer zone when $\varepsilon = 0.999$ and $u = 0.1\ \mu m/s$.

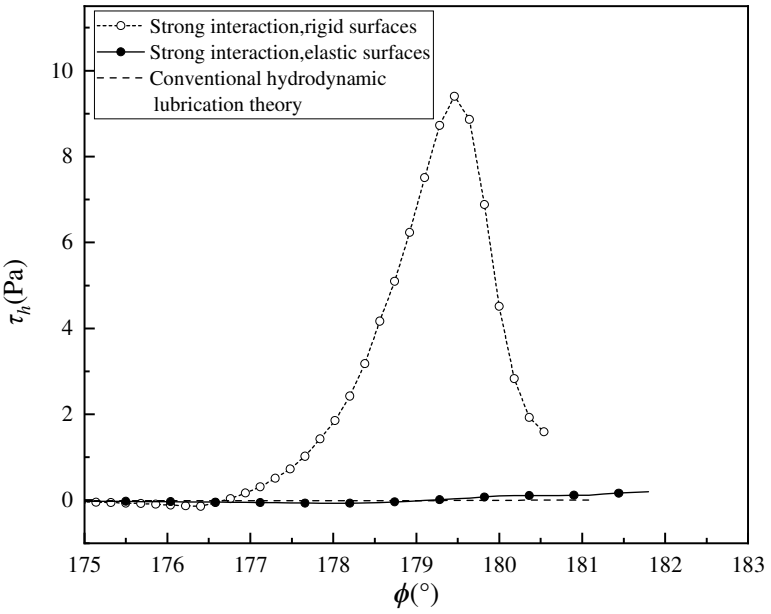
Strong interaction,rigid surfaces
Strong interaction,elastic surfaces
Conventional hydrodynamic lubrication theory
$\tau_h$(Pa)
$\phi$(°)
0
2
4
6
8
10
175
176
177
178
179
180
181
182
183

*(a)*

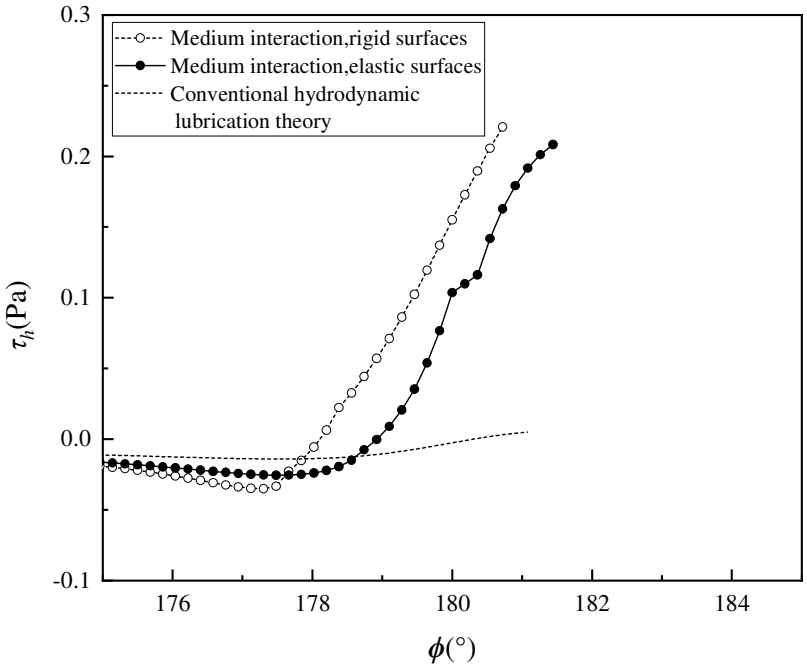
Medium interaction,rigid surfaces
Medium interaction,elastic surfaces
Conventional hydrodynamic lubrication theory
$\tau_h$(Pa)
$\phi$(°)
-0.1
0.0
0.1
0.2
0.3
176
178
180
182
184

*(b)*

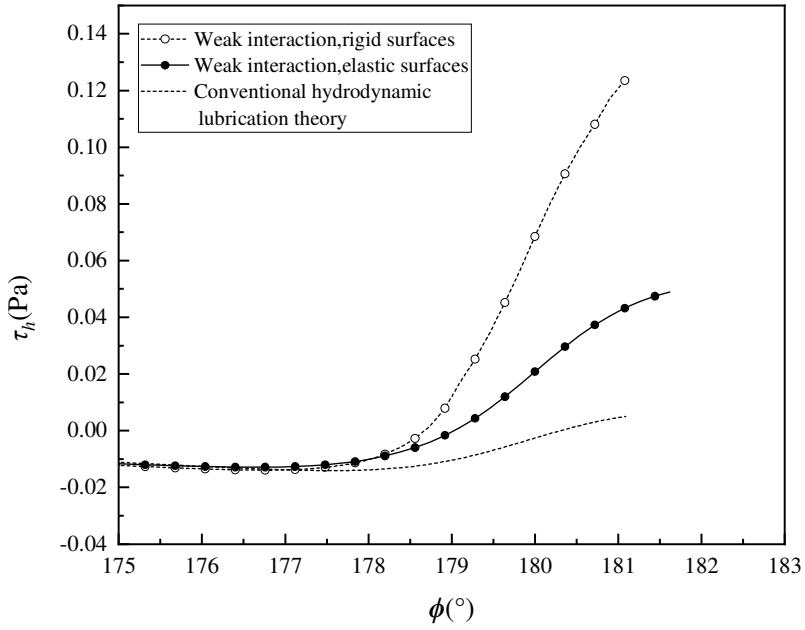


*(c)*

**Fig. 11** *The shear stresses $\tau_h$ on the sleeve in the pure adsorbed layer zone when $\varepsilon = 0.999$ and $u = 0.1$ μm/s*

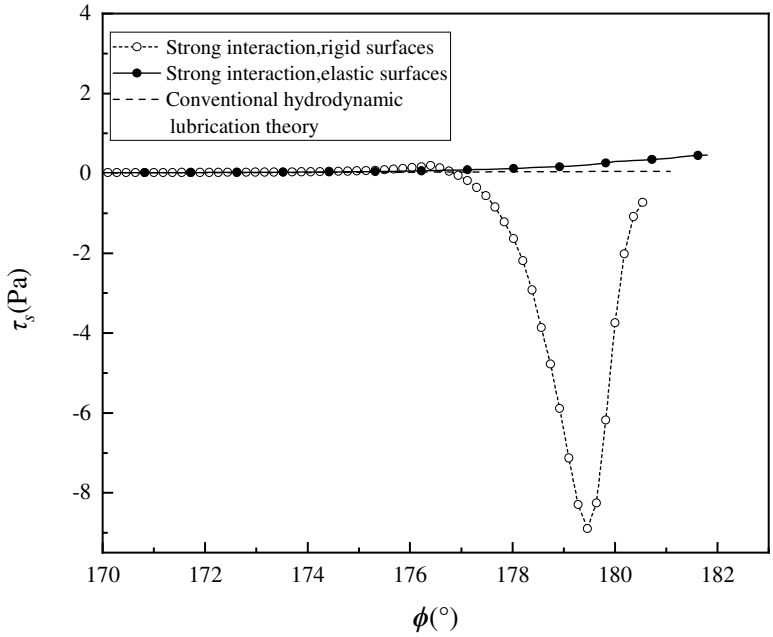


*(a)*

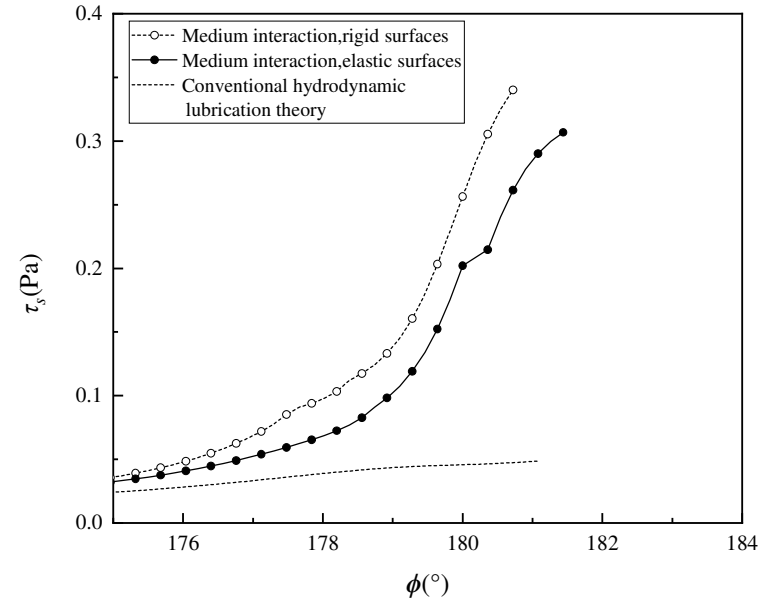


*(b)*

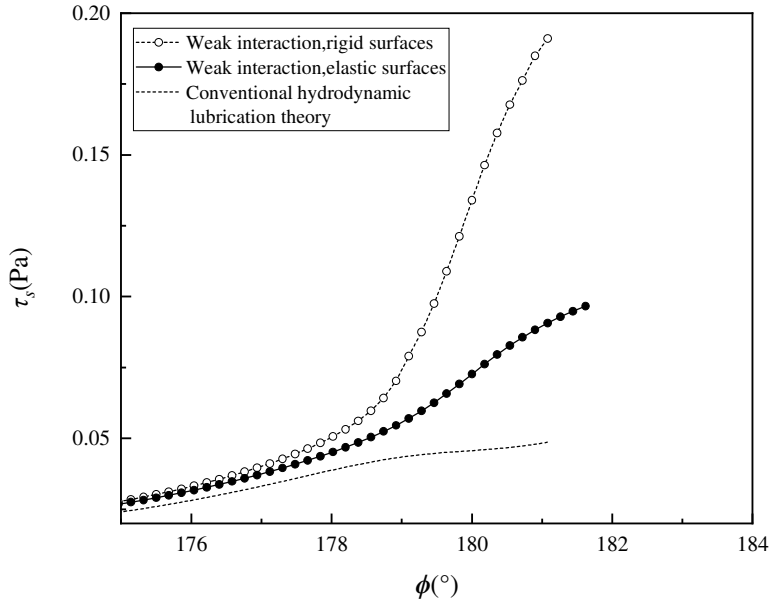


*(c)*

**Fig. 12** *The shear stresses $\tau_s$ on the shaft in the pure adsorbed layer zone when $\varepsilon = 0.999$ and $u = 0.1\ \mu m/s$*

Figures 13(a) and (b) show the friction coefficients on the sleeve and shaft surfaces, respectively, for different contact regimes calculated from the present model and from the classical hydrodynamic lubrication theory [12] when $u = 0.1\ \mu m/s$ and the values of $\varepsilon$ approach unity. The calculated friction coefficients are all very low, on the scales of $10^{-4}$ and $10^{-5}$. When the adsorbed layer effect is considered, the friction coefficients obtained are aproximately half or even less than

those predicted from classical hydrodynamic lubrication theory. For a given $\varepsilon$ and a given fluid-surface interaction, the surface elasticity causes a significant increase in the friction coefficients on both the sleeve and the shaft. Conversely, for a given $\varepsilon$, a stronger fluid-surface interaction results in lower friction coefficients on both the sleeve and the shaft, whether the bearing surfaces are assumed to be rigid or elastically deformed.

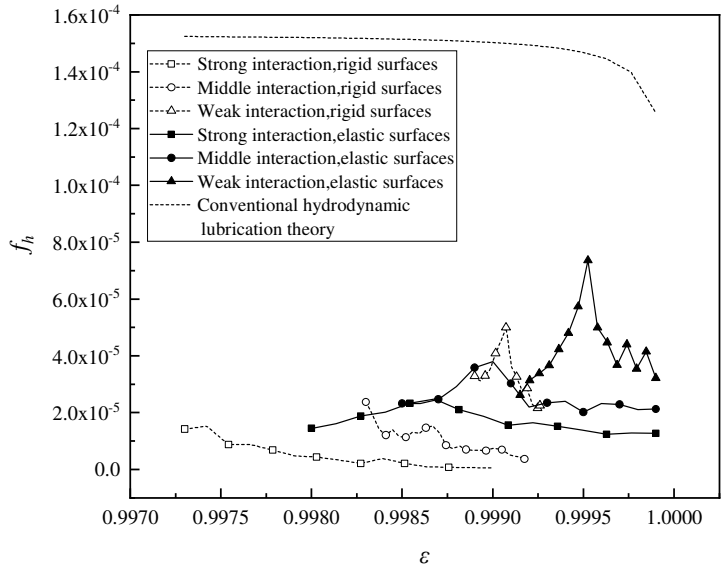


**(a)** *Friction coefficient on the sleeve*

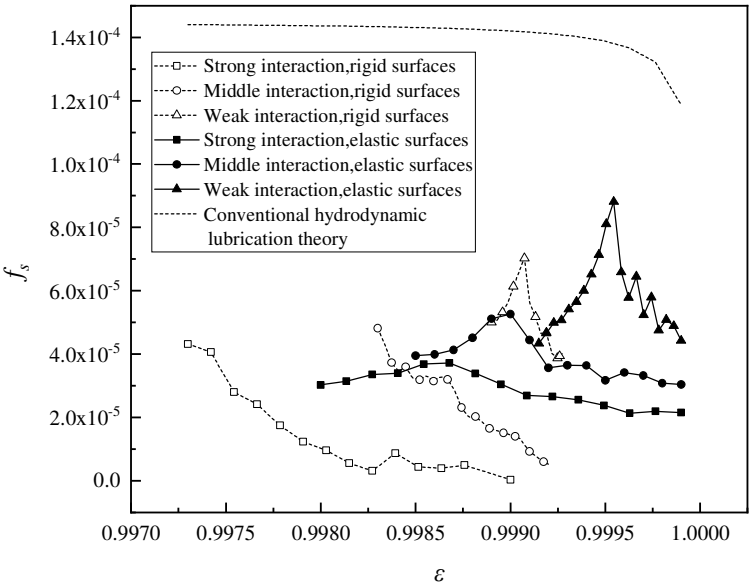


**(b)** *Friction coefficient on the shaft*

**Fig. 13** *Friction coefficients on the sleeve and shaft, respectively, for different contact regimes, obtained using the present model and the classical hydrodynamic lubrication theory [12] when u = 0.1 μm/s and the values of ε approach unity*

## 6. CONCLUSION

The effects of surface elasticity have been included. The governing differential equations were numerically discretized using the forward difference method, and the resulting equations were solved based on the specified boundary conditions.

According to the obtained results, the main conclusions are as follows:

The load and friction performances of the hydrodynamic lubricated journal bearing with ultra-small surface clearances (where the eccentricity ratios approach unity) have been computationally investigated using the multiscale approach. This f bearing regime occurs under conditions of heavy loads, high lubricant temperatures and/or low sliding speeds. In this bearing regime a pure physically adsorbed boundary layer is locally present. The nanoscale non-continuum flow equation has been employed to calculate the flow rate through the pure adsorbed layer zone, while Zhang's multiscale flow equations have been applied to evaluate the total flow rate through the sandwich film region, where both the adsorbed layer and the continuum fluid film coexist. The effects of surface elasticity have been included. The governing differential equations were numerically discretized using forward difference method, and the resulting equations were solved based on the specified boundary conditions.

According to the obtained results, the main conclusions are as follows:

(a) For the given eccentricity ratio and sliding speed, the surface elasticity leads to significant reductions of both the maximum film pressure and the bearing load, particulary under strong fluid-surface interactions.

(b) For a given eccentricity ratio and sliding speed, the surface elasticity results in a notable increase in the surface separations within the pure adsorbed layer zone, including the minimum surface clearance. This effect is especially pronounced for strong fluid-surface interaction.

(c) The film stiffness of the bearing with the elastically deformed surfaces is greater than that of the bearing with the assumed rigid surfaces, particularly when the fluid-surface interaction is strong.

(d) For a given eccentricity ratio and sliding speed, surface elasticity considerably reduces the magnitudes of the shear stresses on both the sleeve and the shaft within the pure adsorbed layer zone, especially for strong fluid-surface interactions. However, it substantially increases the friction coefficients on both surfaces, in contrast to the results for the assumed rigid surfaces.

(e) The influences of the fluid-surface interaction and the sliding speed on the film pressure and bearing load are weaker for elastically deformed surfaces than for assumed rigid surfaces.

(f) Whenever the bearing surfaces are rigid or elastically deformed, stronger fluid-surface interaction lead to higher film pressures and greater bearing load, while simultaneously producing lower friction coefficients on both bearing surfaces.

The obtained results provide the following important implications for the design of the hydrodynamic journal bearing operating with ultra-small surface clearances. The fluid-surface

interaction should be as strong as possible to enhance the load-carrying performance. A bearing surface with a low Young's modulus of elasticity is advantageous for increasing the load capacity of the bearing. However, to achieve lower friction coefficients, a bearing surface with a high Young's modulus of elasticity is preferable.

## NOMENCLATURE

$e$ - eccentricity of the bearing
$h_{bf}$, $h$ - thicknesses of the adsorbed layer and the continuum fluid film, respectively
$h_{tot}$ - surface separation
$R$, $r$ - radii of the sleeve and the shaft, respectively
$u$ - circumferential speed of the shaft
$\phi_e$, $\phi_0$ - angular coordinates of the bearing exit and the location of maximum film pressure, respectively

## 7. REFERENCES

[1] Childs, P.R.N., *Mechanical Design*, Elsevier, 2004.
https://doi.org/10.1016/B978-075065771-6/50003-9

[2] Bukovnik, S., Offner, G., Gaika, V., Priebsch, H.H., Bartz, W.J., Thermo-elasto-hydrodynamic lubrication model for journal bearing including shear rate-dependent viscosity, *Lubrication Science*, Vol. 19, No. 4, pp. 231–245, 2007.
https://doi.org/10.1002/ls.45

[3] Attia, H.M., Bouaziz, S., Maatar, M., Fakhfakh, T., Haddar, M., Hydrodynamic and elastohydrodynamic studies of a cylindrical journal bearing, *Journal of Hydrodynamics*, Vol. 22, pp. 155–163, 2010. https://doi.org/10.1016/S1001-6058(09)60041-X

[4] Gecim, B., Non-Newtonian effects of multigrade oils on journal bearing performance, *Tribology Transactions*, Vol. 33, No. 3, pp. 384-394, 1990.
https://doi.org/10.1080/10402009008981968

[5] Dang, R.K., Goyal, D., Chauhan, A., Dhami, S.S., Effect of non-newtonian lubricants on static and dynamic characteristics of journal bearings, *Materials Today: Proceedings*, Vol. 28, No. 3, pp. 1345-1349, 2020.
https://doi.org/10.1016/j.matpr.2020.04.727

[6] Lee, D., Sun, K.H., Kim, B., Kang, D., Thermal behavior of a worn tilting pad journal bearing: Thermohydrodynamic analysis and pad temperature measurement, *Tribology Transactions*, Vol. 61, No. 6, pp. 1074-1083, 2018.
https://doi.org/10.1080/10402004.2018.1469805

[7] Lorenz, N., Offner, G., Knaus, O., Thermal analysis of hydrodynamic lubricated journal bearings in internal combustion engines, Proceedings of the Institution of Mechanical Engineers, Part K: *Journal of Multi-body Dynamics*, Vol. 231, No. 3, pp. 406-419, 2017. https://doi.org/10.1177/1464419317693878

[8] Maharshi, K., Mukhopadhyay, T., Roy, B., Roy, L., Dey, S., Stochastic dynamic behaviour of hydrodynamic journal bearings including the effect of surface roughness, *International Journal of Mechanical Sciences*, Vols. 142-143, pp. 370-383, 2018. https://doi.org/10.1016/j.ijmecsci.2018.04.012

[9] Jagadeesha, K.M., Nagaraju, T., Sharma, S.C., Jain, S.C., 3D surface roughness effects on transient non-Newtonian response of dynamically loaded journal bearings, *Tribology Transactions*, Vol. 55, No. 1, pp. 32-42, 2012. https://doi.org/10.1080/10402004.2011.626144

[10] Hase, A., Mishina, H., Wada, M., Fundamental study on early detection of seizure in journal bearing by using acoustic emission technique, *Wear*, Vols. 346-347, pp. 132-139, 2016. https://doi.org/10.1016/j.wear.2015.11.012

[11] Zhang, Y.B., Modeling of flow in a very small surface separation, *Applied Mathematical Modelling*, Vol. 82, pp. 573-586, 2020. https://doi.org/10.1016/j.apm.2020.01.069

[12] Pinkus, O., Sternlicht, B., *Theory of hydrodynamic lubrication*, McGraw-Hill, New York, 1961.

[13] Shao, S.J., Zhang, Y.B., Chen, L., Jiang, X.D., Multiscale hydrodynamic journal bearing with ultra-low surface separation, *International Journal of Automotive Technology,* Vol. 23, pp. 1691-1702, 2022. https://doi.org/10.1007/s12239-022-0147-2

[14] Zhang, Y.B., The flow equation for a nanoscale fluid flow, *International Journal of Heat and Mass Transfer*, Vol. 92, pp. 1004-1008, 2016. https://doi.org/10.1016/j.ijheatmasstransfer.2015.09.008

[15] Zhang, Y.B., Flow factor of non-continuum fluids in one-dimensional contact, *Industrial Lubrication and Tribology*, Vol. 58, No. 3, pp. 151-169, 2006. https://doi.org/10.1108/00368790610661999

[16] Zhang, Y.B., The flow factor approach model for the fluid flow in a nano channel, *International Journal of Heat and Mass Transfer,* Vol. 89, pp. 733-742, 2015. https://doi.org/10.1016/j.ijheatmasstransfer.2015.05.092